IEEE Access
Multidisciplinary ⋮ Rapid Review ⋮ Open Access Journal

Received February 25, 2021, accepted March 27, 2021, date of publication April 7, 2021, date of current version April 16, 2021.

Digital Object Identifier 10.1109/ACCESS.2021.3071515

Evidence-Theoretic Reentry Target Classification Using Radar: A Fuzzy Logic Approach

KWANGYONG JUNG[1], SAWON MIN[2], JEONGWOO KIM[2], NAMMOON KIM[2], AND EUNTAI KIM[1], (Member, IEEE)

[1]School of Electrical and Electronic Engineering, Yonsei University, Seoul 03722, South Korea
[2]Land Radar Team, Radar System Center, Hanwha Systems Company Ltd., Yongin 17121, South Korea

Corresponding author: Euntai Kim (etkim@yonsei.ac.kr)

ABSTRACT This study focuses on the reentry target classification and fuses target features based on the generalized evidence theory. The features are extensively investigated, and the ballistic factor and length of the high-resolution range profile are selected. The evidence theory is advantageous for solving feature fusion, representing uncertainty, and is widely used in defense applications. However, determining the generalized basic probability assignment (GBPA) and dealing with uncertainty is a matter that requires further improvement. In this paper, we propose a new method to determine GBPA using uncertainty with time-series radar data. First, the samples of each known class are encoded as a generalized fuzzy number (GFN), and the power set comprising the frame of discernment (FOD) is calculated from the GFN and each intersection area. Subsequently, the test samples with uncertainty are encoded as triangular fuzzy numbers, reflecting the mean and standard deviation of a Kalman filter. Finally, the firing strength between the model and the input is calculated as the degree of support for the class hypothesis, which is used to determine the GBPA. The proposed algorithm is compared with the existing methods and exhibits high classification accuracy and a short classification time without leakage. In experiments with various input uncertainties, the results demonstrate that our method can effectively reflect the input uncertainty and determine the GBPA.

INDEX TERMS Basic probability assignment, Dempster-Shafer evidence theory, generalized evidence theory, generalized fuzzy number, reentry target classification.

I. INTRODUCTION

Ballistic missile defense (BMD) systems aim at intercepting warheads during the boost, mid-course, and reentry phases of their trajectories. In BMD, warhead classification is great importance because it significantly affects the success rate of warhead interception. Leakage, which classifies warheads as different targets, is a fundamental reason for interception failure. In contrast, a false alarm that incorrectly classifies debris, decoys, or boosters as warheads may lead to a waste of the interceptor resource and hinder further warhead engagement [1]. Currently, the success rate of intercepts has been reported to be slightly higher than half in ground-based mid-course defense [2]. To improve this success rate, warheads should be intercepted again during the reentry phase. Multi-function radar (MFR) is a key sensor for searching, tracking, and engaging multiple hostile targets simultaneously in BMD systems [3]. This study focuses on the reentry target classification task of the MFR to prevent leakage and false alarms.

The main difficulties in warhead classification arise from two aspects. First, the sensor data from radar contain uncertainties due to measurement errors and the environment, as well as a lack of relevant knowledge. These uncertainties provide conflicting evidence, thereby complicating the classification task [4]. Second, classification needs to be performed within a significantly short period due to the low altitude and high speed of warheads [5]. This time constraint makes it difficult to use features that require a long time for extraction.

Numerous studies focusing on warhead classification have been conducted in the last decade. Classification methods using feature matching [6], [7], the hidden Markov model [8], and the Dempster–Shafer evidence theory (D–S theory) [9], [10] were studied to utilize the target kinematic parameters of the narrowband feature. The support vector machine (SVM) and neural network (NN) were used in [11], [12] to utilize the radar cross section (RCS). For methods using wideband features, the k-nearest neighbor (kNN) was applied

The associate editor coordinating the review of this manuscript and approving it for publication was Chengpeng Hao.

to use high-resolution range profiles (HRRPs) in [1], [13]. The results of the SVM and convolutional neural network (CNN) were compared using histograms of oriented gradient (HOG) features of HRRP in [14]. Warhead classification studies using micro-Doppler (mD) feature have also been conducted [5], [15], [16]. It should be noted that most of these previous works focused on using narrowband or wideband features separately, and time-consuming classification methods may not be suitable during the reentry phase.

In contrast, the D–S theory is considered as a possible solution to fuse selected features and overcome the time constraint. The main advantage of the D-S theory is that it can assign probabilities to each interval or set of individual evidence. Moreover, multi-source information can be fused without a prior probability distribution [17]. The D-S theory offers a mathematical framework for uncertainty modeling [18]. Moreover, the D-S theory can decrease the degree of uncertainty [19]. Notably, the D-S theory has been applied to warhead and ballistic missile classification in several studies. Warhead classification ability was tested by merging the test data collected by two infrared sensors in [4]. The D-S theory was applied to deal with limited a priori data and short observation times for the purpose of ballistic missile classification with radar data in [9]. This theory has also been studied to classify ballistic missiles as a framework to fuse multi-sensor information in [20]. As an extension of the D-S theory, the generalized evidence theory (GET) can deal with uncertain information. The GET offers the concept of the generalized basic probability assignment (GBPA) and generalizes the D-S theory in the open world [21]. In the GET, unknown targets can be represented as an empty set [22], [23]. The conflict coefficient, which indicates a conflict of evidence, can also provide useful information for expressing uncertain targets. Nevertheless, the evidence theory still has some room to exploit when it is applied to the warhead classification via radar.

First, a unified methodology for assigning basic probability (BP) to each proposition has not been fully developed. Many researchers have proposed different methods for assigning BP as follows: non-parametric [24], kernel distribution [25], normal distribution [26], k-mean clustering [27], and fuzzy theory [10], [28]. In the past few years, some studies have used a generalized fuzzy number (GFN) [29], a trapezoidal fuzzy number [30], and a triangular fuzzy number (TFN) [17], [19], [22], [31] methods to improve classification performance. Various approaches have been compared to explain the conflict between the evidence, but some applications still require improvement [32]. Recent research efforts have also been devoted toward determining GBPA in the open world [17], [19], [21], [22].

Second, most previous works have not considered methods to deal with the uncertainty in time series data. An incomplete frame of discernment (FOD) and uncertainty of sensor measurements are the two main causes of conflicting evidence [21], [23]. The GET can effectively deal with the incomplete FOD in the open world. However, test samples are treated as a single deterministic value, and the input uncertainty is not taken into consideration when assigning basic probability [17], [22], [31]. Therefore, if the data collected in a noisy environment are not accurate, further improvement is needed.

In this paper, we propose a novel approach to determine GBPA using the uncertainty with time-series radar data. First, the propositions of the power set are encoded as GFN using training samples of each known class. Second, the time-series test samples estimated by a Kalman filter (KF) [33], [34] are encoded as TFNs using the mean and standard deviations. The covariance of the KF reflects the process noise and measurement noise of the radar. In this step, the radar input uncertainty is reflected in the TFN. If the standard deviation is sufficiently small or ignored, it is encoded as TFN with only the center value. At this time, the proposed method also features downward compatibility with existing methods. Finally, the degree of support is calculated to determine GBPA using the intersection of GFN and TFN.

The primary contributions of this paper are as follows:

1) A novel method is proposed to determine the GBPA; this method uses the mean and covariance of the KF of the MFR. Unlike previous studies, the uncertainty of time-series features are effectively reflected during the assignment of basic probabilities.
2) The proposed method uses both narrowband and wideband features in real-time. Not all time-series data need to be stored for matching or classification.

The remainder of this paper is organized as follows. Related works are presented in Section II. Section III introduces the basic background. In Section IV, we propose a novel method to determine GPBA. In Section V, a few numerical examples are presented to understand the procedure. Section VI presents the simulation results of the proposed algorithm. Finally, the analysis results and the excellent performance of the proposed algorithm are described in Section VII.

II. RELATED WORKS

This section reviews previous works with an emphasis on narrowband and wideband features, which are complementary. For example, narrowband features provide kinematic information, while wideband features can improve classification through detailed target information. Suitable features have, therefore, been selected for classification.

A. NARROWBAND FEATURES

Studies have been conducted using the following features: acceleration differences [6], aerodynamic properties [7], acceleration, height and specific energy [8], velocity, energy height and flight angle [9], position, velocity, RCS and acceleration [11], and dynamic RCS sequence [12]. However, several features have similar characteristics at a certain altitude or below during the reentry phase. Consequently, there may be contradictory features that reduce the classification

performance. In contrast, the ballistic factor (BF) can extract reentry characteristics suitably. Compared to warheads, which are designed to have low atmospheric deceleration, intercepted debris have lighter weights and irregular shapes. Thus, it is possible to distinguish between warheads and debris based on the lower speed of the latter, caused by drag [1], [35]. We, therefore, use the BF to distinguish between the movements of warheads, debris, and other objects.

B. WIDEBAND FEATURES

The wideband features used for classification are mD and HRRP. The mD image is difficult to use during the reentry phase because more than a few seconds are required to process the signal. The processing time of HRRP is shorter than that of mD because of using the one-dimensional amplitude of the radar target echo. However, the HRRP template matching method requires a significant amount of storage and exerts a high computational burden [36]. If the features are not extracted appropriately owing to the irregular shapes of debris, target postures, and maneuvering, guaranteeing classification performance becomes difficult. The target length is a good alternative to compensate for these shortcomings. Studies have been conducted to estimate the warhead length based on HRRP [37]–[39]. During reentry, warheads tend to be better aligned and more stable along the direction of the velocity vector, in order to ensure that they do not deviate from the trajectory; this is not the case for intercepted debris or other similar objects [1], [40]. Therefore, the length of the warhead can be measured more reliably than other objects. The proposed method uses irregular length measurement features of debris or other objects that fly irregularly, even if the target length is not extracted precisely.

III. PRELIMINARIES

A. DEMPSTER-SHAFER EVIDENCE THEORY

1) FRAME OF DISCERNMENT

D-S Theory was proposed by Dempster [41] and later improved by Shafer [42]. In D-S theory, a set of all possible hypotheses is called FOD (Θ) and it is defined as

$$\Theta = \{\alpha_1, \alpha_2, \ldots, \alpha_l, \ldots, \alpha_N\} \tag{1}$$

The FOD consists of the hypothesis that N elements are mutually exclusive. $P(\Theta)$ is a power set of Θ which is defined by

$$P(\Theta) = \{\emptyset, \alpha_1, \alpha_2, \ldots, \alpha_N, \{\alpha_1, \alpha_2\}, \{\alpha_1, \alpha_3\} \ldots, \{\alpha_2, \ldots, \alpha_l\}, \ldots, \Theta\} \tag{2}$$

where, $\emptyset$ denotes empty set. $P(\Theta)$ has 2^N propositions of Θ.

2) BASIC PROBABILITY ASSIGNMENT

The BPA, which is termed as a mass function m, maps the elements(α) of the FOD to a probability in [0, 1] as

$$m : P(\Theta) \rightarrow [0, 1] \tag{3}$$

which satisfies the following conditions:

$$\sum_{\alpha \in P(\Theta)} m(\alpha) = 1 \tag{4}$$

$$0 \leq m(\alpha) \leq 1 \quad \forall \alpha \in P(\Theta) \tag{5}$$

$$m(\phi) = 0 \tag{6}$$

The function m(α) represents the degree to which the evidence supports proposition α. If the value of m(α) is not zero, then α is a focal element.

3) RULE OF COMBINATION

Next, define the probability mass assigned by two different attributes as m_1 and m_2 that support different propositions. If the focal elements of m_1 and m_2 are α_i and α_j, respectively, new $m(\alpha)$ is combined by the combination rule as follows:

$$m(\alpha) = \frac{q(\alpha)}{1 - q(\phi)} \quad \forall \alpha \neq \phi \tag{7}$$

$$q(\alpha = \sum_{\forall i,j \alpha_i \cap \alpha_j = \alpha} m_1(\alpha_i) \cdot m_2(\alpha_j) \tag{8}$$

where, $q(\emptyset)$ denotes the conflict between two BPAs. A larger value indicates more conflicting the information regarding the attributes, and get limited information after combination [26]. Therefore, this should be handled carefully [43].

4) PIGNISTIC PROBABILITY

The pignistic probability is proposed to determine the final decision [44]. The function $BetP : \Theta \rightarrow [0, 1]$ is defined by

$$BetP(\alpha_i) = \sum_{\alpha_j \subseteq \Theta} \frac{|\alpha_i \cap \alpha_j|}{|\alpha_j|} \cdot \frac{m(\alpha_j)}{1 - m(\emptyset)} \quad \forall \alpha_i \subseteq \Theta \tag{9}$$

where, $m(\emptyset) \neq 1$ and $|X|$ is the cardinality of set X.

B. GENERALIZED EVIDENCE THEORY

The GET is proposed by Deng [21] for handling incomplete FOD. It can be applied by extending the traditional evidence theory for the case where $m(\emptyset) \neq 0$. In the case of $m(\emptyset) = 0$, the GET is degenerated to traditional evidence theory [19]. Some basic definitions of GET are as follows:

1) GENERALIZED BASIC PROBABILITY ASSIGNMENT

Suppose that U is a FOD. The power set composed of 2^U propositions is denotes 2^U_G, $\forall A \subset U$. A GBPA is a mass function that maps $m_G : 2^U_G \rightarrow [0, 1]$ that satisfies [21]:

$$\sum_{A \in 2^U_G} m_G(A) = 1 \tag{10}$$

The GET has no restriction that $m_G(\emptyset)$ should be zero. Therefore, the empty set is a focal element.

2) GENERALIZED COMBINATION RULE

The generalized combination rule (GCR) between two given GBPA is defined as follows [21]:

$$m(A) = \frac{(1 - m(\emptyset)) \sum_{B \cap C = A} m_1(B) m_2(C)}{1 - K} \tag{11}$$

with

$$K = \sum_{B \cap C = \emptyset} m_1(B) m_2(C) \tag{12}$$

$$m(\emptyset) = m_1(\emptyset) m_2(\emptyset) \tag{13}$$

$$m(\emptyset) = 1 \quad \text{if and only if} \quad K = 1 \tag{14}$$

C. FUZZY SET THEORY

The fuzzy theory, proposed by Zadeh [45], has been successfully applied in various applications. Some necessary background of fuzzy set and fuzzy numbers are given as follows:

1) GRADE OF MEMBERSHIP

Let X be a universal set. The membership function $\mu_A(x)$ maps each elements of the fuzzy set A with real numbers in the interval [0, 1].

$$\mu_A : X \to [0, 1] \tag{15}$$

2) BASIC OPERATION

For two fuzzy sets A and B, the intersection C is an AND operation, and is defined as follows:

$$\mu_C(x) = min(\mu_A(x), \mu_B(x)) \tag{16}$$

3) GENERALIZED FUZZY NUMBER

A membership function of GFN $\widetilde{A} = (a, b, c, d; w)$, where $a \le b \le c \le d$ and $0 < w < 1$, is defined as follows [46]:

$$\mu_{\widetilde{A}}(x) = \begin{cases} 0, & x < a; \\ w\dfrac{x-a}{b-a}, & a \le x \le b; \\ w, & b \le x \le c; \\ w\dfrac{d-x}{d-c}, & c \le x \le d; \\ 0, & x > d; \end{cases} \tag{17}$$

Because of the parameter w that represents the degree of confidence, GFN can handle uncertain information more flexibly than normal fuzzy number [47]. If $w = 1$, $\widetilde{A}$ is a trapezoidal fuzzy number. If $a = b$ and $c = d$, $\widetilde{A}$ is a crisp interval. If $b = c$, $\widetilde{A}$ is a triangular fuzzy number (TFN). If $a = b = c = d$ and $w = 1$, $\widetilde{A}$ is real number. The difference between a traditional fuzzy number and a GFN is that the height of a traditional fuzzy number is equal to 1, but the height of a GFN is between 0 to 1. If w differs in each interval, A is generalized trapezoidal fuzzy number with different left and right heights. Additional details can be found in [48], [49].

D. TARGET FEATURES

1) BALLISTIC FACTOR

The main characteristic of the reentry phase target is rapid deceleration due to air density in the atmosphere. The BF of the target determines drag acceleration in the atmosphere, as follows:

$$\ddot{\vec{r}} = -\frac{C_x S}{m} \frac{\rho(H)}{2} \vec{v} \tag{18}$$

where C_x is generally a drag coefficient according to the shape and speed of the target. S is the cross section area of the target (m^2). m is the mass (kg) of the target. $\rho(H)$ is the atmospheric density (kg/m^3) according to the altitude of the target. $\vec{v}$ is the speed of the target (m/s). In some studies, $\beta = m/C_x S$ is defined as the ballistic coefficient and is used for trajectory modeling [50]. In this study, the BF (m^2/kg) is defined as follows:

$$\gamma = \frac{C_x S}{m} \tag{19}$$

The typical BF of a warhead ranges from 1×10^{-4} to 5×10^{-4} m^2/kg, whereas that of debris is 0.01–0.1 m^2/kg [35]. The equation of theoretical atmospheric density $\rho(H)$ is expressed as follows [51]:

$$\rho(H) = \begin{cases} 1.219 \times e^{-\frac{h}{9146.640}}, & h < 9146.64 \text{ (m)} \\ 1.754 \times e^{-\frac{h}{6707.536}}, & h > 9146.64 \text{ (m)} \end{cases} \tag{20}$$

In this study, the target-specific ballistic coefficient for initializing the trajectory is assumed to remain constant in the overall scenario trajectory modelling.

2) TARGET LENGTH FROM HRRP

To estimate the target length, RCS analysis and scatter point extraction are performed as follows:

- Computer-aided design (CAD) model: With reference to ballistic missile targets [52] and similar experience [39], CAD models for targets were built.
- Analysis of RCS using computational electromagnetic method tool: Physical optics (PO) and shooting-and-bouncing-rays (SBR) techniques were implemented to calculate the RCS.
- Scattering center extraction: The scatter point is extracted using the MUSIC algorithm [53].
- Target length estimation: The scatter point extraction result is used to estimate target length according to the line of sight (LOS).

The target length (L) can be estimated as follows [39]:

$$L = \frac{L_r}{\cos\phi} \tag{21}$$

The length L_r in the direction of $\vec{r}$ can be obtained from the HRRP extracted from the receiving signal. The warhead heading is well aligned with the velocity vector $\vec{v}$ during the reentry phase. [40]. Therefore, the angle between the heading and the LOS of the radar is defined as follows:

$$\cos\phi = \frac{\vec{r} \cdot \vec{v}}{|\vec{r}| \cdot |\vec{v}|} \tag{22}$$

The method of estimating the target length may include errors if L_r is not estimated appropriately. In addition, the estimated length fluctuates significantly for non-warhead targets due to random rotation. In this study, we use the estimated length measures.

IV. PROPOSED METHOD

The existing radar samples with n classes are divided into two sets: a training set and a test set. The training set is used to construct the GFN, and the test set is used to construct the TFN and then obtain the GBPA using the proposed method. A sample of each class has k attributes. The k attributes support propositions that represent mutually exclusive target classes. The process of determining GBPA is described as follows:

A. STEP 1: ENCODE POWER SET TO GFN

In this step, the propositions (α_i) are encoded to GFN. $\mu^k_{\widetilde{\alpha}_i}(x)$ is defined as a membership function (MF) in i^{th} proposition of k^{th} attribute. First, each MF is calculated for the n class in FOD. Subsequently, MFs are calculated for all propositions through the fuzzy intersection operation in (16). The number of propositions m is calculated as follows:

$$m = 2^n = \sum_{j=0}^{n} \frac{n!}{(n-j)!j!} \tag{23}$$

We assume that there are three target classes in the FOD. Each $\mu^k_{\widetilde{\alpha}_i}(x)$ is defined as follows:

$$\mu^k_{\widetilde{\alpha}_0}(x) = 0 \tag{24}$$
$$\mu^k_{\widetilde{\alpha}_1}(x) = \mu^k_{\widetilde{\alpha}_1}(x) \tag{25}$$
$$\mu^k_{\widetilde{\alpha}_2}(x) = \mu^k_{\widetilde{\alpha}_2}(x) \tag{26}$$
$$\mu^k_{\widetilde{\alpha}_3}(x) = \mu^k_{\widetilde{\alpha}_3}(x) \tag{27}$$
$$\mu^k_{\widetilde{\alpha}_4}(x) = min(\mu^k_{\widetilde{\alpha}_1}(x), \mu^k_{\widetilde{\alpha}_2}(x)) \tag{28}$$
$$\mu^k_{\widetilde{\alpha}_5}(x) = min(\mu^k_{\widetilde{\alpha}_1}(x), \mu^k_{\widetilde{\alpha}_3}(x)) \tag{29}$$
$$\mu^k_{\widetilde{\alpha}_6}(x) = min(\mu^k_{\widetilde{\alpha}_2}(x), \mu^k_{\widetilde{\alpha}_3}(x)) \tag{30}$$
$$\mu^k_{\widetilde{\alpha}_7}(x) = min(min(\mu^k_{\widetilde{\alpha}_1}(x), \mu^k_{\widetilde{\alpha}_2}(x)), \mu^k_{\widetilde{\alpha}_3}(x)) \tag{31}$$

The MF of empty set is shown in (24). The MFs corresponding to n classes are shown in (25)–(27). The MFs for the remaining propositions are shown in (28)–(31).

We propose two methods to determine the GFN for n classes. To reflect the characteristics of a data set in which data converge to a steady-state region, the GFN encoding method is modified as follows:

1) Use existing training data of the minimum (Min), maximum (Max) values that contain the k^{th} attributes of the i^{th} target classes [29].
2) Split and select time series data to include the steady-state region (χ_S). Let x_s be $x_s \in \chi_S$. For example, the x_s can be bounded by typical values.
3) Select the lower bound (lb^k_i) and the upper bound (ub^k_i) of x_s instead of average.
4) GFN is defined as $\widetilde{\alpha}_i = (Min^k_i, lb^k_i, ub^k_i, Max^k_i; 1)$.

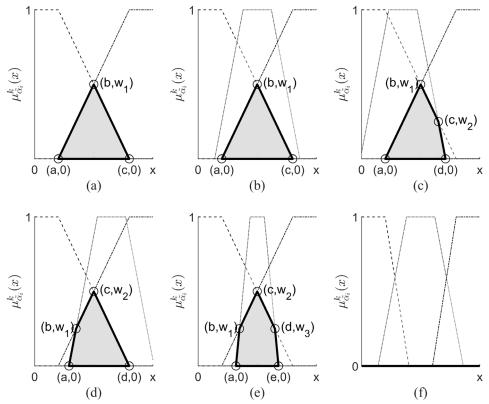

FIGURE 1. The intersection between two GFN.

The mean and standard deviation of the time-series data that converge to a steady-state over time, such as the BF, exhibit a time-varying property. Based on experience, expressing the data in GFN is more representative of the distribution of data than expressing it in TFN.

For a simpler data set, such as the length, the GFN encoding method is modified as follows:

1) Use existing sample data of the Min, Max values that contain the k^{th} attributes of the i^{th} target classes [29].
2) Plot a histogram in class of each attributes, overlaid with a plot of the probability distribution function of the fitted distribution, by using log-normal distribution function.
3) Select the point of the global maximum ($mode^k_i$) by using $e^{(\mu-\sigma^2)}$.
4) GFN is defined as $\widetilde{\alpha}_i = (Min^k_i, mode^k_i, Max^k_i; 1)$.

The center value of TFN can be determined using the mean [17], [22], k-means++ clustering [31]. However, the length measurements are limited by radar resolution. Some results with a strong signal are measured to be longer than their actual length. In addition, the radar cannot obtain measurements smaller than its resolution. Thus, we used the log-normal distribution owing to finite or limited measures.

To provide redundancy to the model, the boundaries can be modified [17]. In this study, we define σ_m by multiplying the radar measurement error with a proportional constant. This allows flexible reflection of changes in radar errors. We use the modified boundary, as follows:

$$Min^k_i = Min^k_i \pm \sigma_m, \quad Max^k_i = Max^k_i \pm \sigma_m \tag{32}$$
$$lb^k_i = lb^k_i \pm \sigma_m, \quad ub^k_i = ub^k_i \pm \sigma_m \tag{33}$$

Subsequently, the GFNs by intersection of two GFN are calculated by using (24), (28)–(31). Fig. 1 represents the possible intersection area of $\mu^k_{\widetilde{\alpha}_i}(x)$ for the generalized trapezoidal fuzzy number. The generated power set membership function is shown in Fig. 1-(a) to Fig. 1-(e). The case of an empty set is represented in Fig. 1-(f). A method of generating a GFN by the intersection of two TFN was proposed in [43].

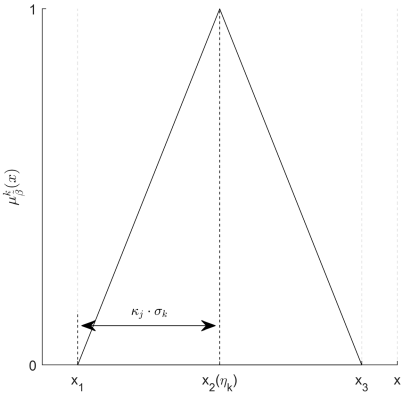

FIGURE 2. The encoded test input as TFN.

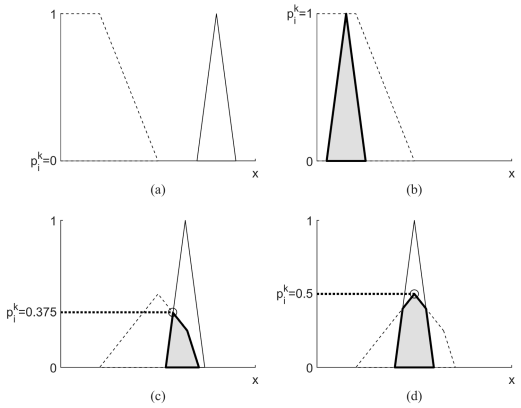

FIGURE 3. The intersection area between GFN and TFN.

B. STEP 2: ENCODE REAL-TIME INPUT TO TFN

In this step, the time-series test samples estimated by the KF, which is used in the radar, are encoded to TFN. Let η_k be the mean and σ_k be the standard deviation for the k^{th} attribute. The membership function is defined as $\mu_{\tilde{\beta}}^{k}(x)$. The method of constructing a TFN using the input of real-time radar measurement values is shown in Fig. 2. To determine corresponding TFN model boundary, the mean and standard deviations are taken into account, as follows:

$$x_j = \eta_k + \kappa_j \cdot \sigma_k, \quad j = 1, 2, 3; \tag{34}$$

where, the proportional coefficient consists of $\kappa_1 = -1, -2, -3$, $\kappa_2 = 0$, $\kappa_3 = 1, 2, 3$. If $x_j \leq 0$, we set $x_j = 0$. This prevents incorrect calculations such as a negative length. If σ_k is ignored or $\sigma_k \leq \epsilon_k$, we set $\kappa_1 = \kappa_3 = 0$. At this time, TFN is a real number. In this case, the proposed algorithm behaves similarly to the existing methods that uses intersection points with a single sample [17], [22], [31]. In this study, we use $\epsilon_k = 1 \times 10^{-4}$ for length, $\epsilon_k = 1 \times 10^{-10}$ for BF.

C. STEP 3: DETERMINING MAXIMUM VALUE BETWEEN GFN AND TFN

In this step, we use the maximum value of the intersection area between the input MF and power set MF. Let p_i^k be the individual firing strength in the i^{th} proposition of the k^{th} attribute. Fig. 3 shows that the firing strength p_i^k measures the degree to which the proposition matches the inputs. This reflects how strongly the input evidence supports each proposition of power set. For the k^{th} attribute, the membership function of intersection area is calculated as follows:

$$\mu_{\tilde{\gamma}_i}^{k}(x) = min(\mu_{\tilde{\alpha}_i}^{k}(x), \mu_{\tilde{\beta}}^{k}(x)), \quad i = 1, 2, \ldots, m \tag{35}$$

p_i^k is the maximum value of $\mu_{\tilde{\gamma}_i}^{k}(x)$, and it is defined as

$$p_i^k = m(\alpha_i^k) = max(\mu_{\tilde{\gamma}_i}^{k}(x), \epsilon_0), \quad i = 1, 2, \ldots, m \tag{36}$$

where, ϵ_0 is the coefficient for preventing computation problem for a complete FOD. In a closed world, if we assign $p_i^k = 0$ when $x \notin [Min_i^k, Max_i^k]$, it would likely conflict with other attributes [24]. We assume $\epsilon_0 = 0$ for the open world and $\epsilon_0 = 0.0001$ for the closed world without affect on the final result.

D. STEP 4: GENERALIZED BASIC PROBABILITY ASSIGNMENT

In this process, one class supported by the largest p_i^k is selected, and the rest are arranged to form a nested structure. For the k^{th} attribute, the procedure to determine GBPA is described in Algorithm 1. At this time, p_i^k corresponding to a proposition with a small number of elements among the same p_i^k values is removed. The proposed method effectively yields a GBPA for a proposition that contains many elements. This is

Algorithm 1 Proposed Method (Pseudo-Code)

Require: $\forall p_i^k \neq \epsilon_0, \quad i = 1, 2, \ldots, N$
  N is number of class in FOD,
  m is number of propositions in power set
Ensure: The GBPA $m(\alpha_i^k)$
  STEP 1: Find maximum value of $p_i^k, \quad i = 1, 2, \ldots, N$
  $p_{max} = max(p_i^k)$
  for $n = 1$ to N **do**
    if $(p_n^k \neq p_{max})$ **then**
      $p_n^k = \epsilon_0$;
    end if
  end for
  STEP 2: Remove conflicts
  for $n = N + 1$ to $m - 1$ **do**
    for $l = N + 1$ to $m - 1$ **do**
      if $(l > n)$ **then**
        if (isequal(p_n^k, p_l^k)) **then**
          $p_n^k = \epsilon_0$;
        end if
        $m(\alpha_n^k) = p_n^k$;
      end if
    end for
  end for
  return $m(\alpha_i^k)$

because the propositions in (2) are already sorted in ascending order by cardinality. This means that the removed proposition is always a subset of the selected proposition. Therefore, the nested structure is formed based on the selected class after normalization. To satisfy (10), if the sum of GPBA is greater than or equal to 1, the final GBPA is $m(\alpha_i^k)/\sum_{i=1}^{m} m(\alpha_i^k)$ and $m(\emptyset) = 0$. In this case, the proposition with a high degree of support is very likely the class in FOD [17]. If the sum of GBPA is less than 1, $m(\emptyset)$ will be assigned as $1 - \sum_{i=1}^{m} m(\alpha_i^k)$ [17], [19].

E. STEP 5: COMBINE GBPA AND DECISION MAKING

In this final step, the GBPA is combined using (11)–(14). For practical applications, we define the decision rule through the following processes. The combined GBPA can be input to the command and control (C2) system for decision-making. If $q(\emptyset) \neq 1$, the pignistic probabilities are used to obtain the target class label [21] and reported with the combined GBPA. In this case, we assume that FOD is complete and GCR is the same as the D-S combination rule when $m(\emptyset) = 0$. We also allow weak conflicts in dealing with the evidence. In this case, the proposition which has the largest value in the combined GBPA can be selected as class label [17]. The the GBPA with the conflict coefficient (K) is reported to C2. We believe that this is useful for real-world applications. In contrast, if the target length cannot be measured due to low signal power or radar resolution, then $m(\emptyset) = 1$. This means that the FOD is highly incomplete. In this case, the GBPAs can be reported without class label. This allows C2 to identify the tracking quality of the target and postpone final decision.

V. NUMERICAL EXAMPLES

In this section, we represent numerical examples to determine the new GBPA using the proposed method.

A. DATA SET

The data set contains three classes: Warhead (W), Booster (B), Debris (D). This data set has 6,462 sample instances each for two attributes: ballistic factor (BF), length (L). These were simulated using the method described in Section III. Table 1 presents the parameters of the target. Each scenario contained trajectories of warheads, boosters, and debris between 10 km to 75 km in altitude. The length attribute contained results that were simulated and found to be longer than the actual target length owing to the signal to noise ratio and signal processing results. The heavy decoy parameter was not used to construct the data set; instead, it was used for the open world experiments. The total number of trajectory scenarios was 45.

B. PROCEDURE

The following conditions were used in experiments. First, 36 scenarios including 6,002 instances were randomly selected as training data to construct the GFN model. The remaining eight scenarios were used as test data. Fig. 4 shows the estimated BF according to altitude, and the values converge to a specific value at low altitude. Fig. 5 shows the estimated L of each target class.

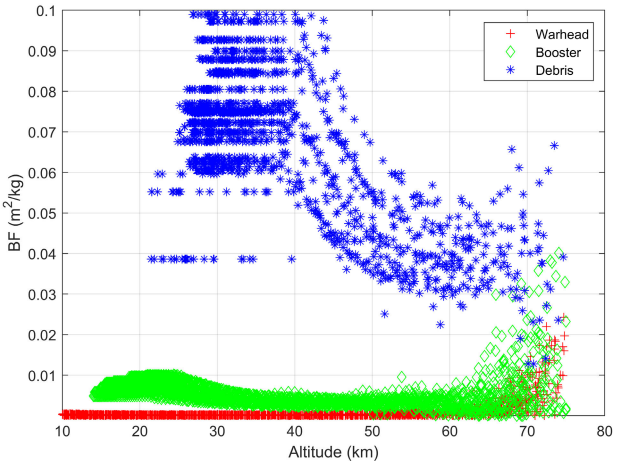

FIGURE 4. Estimated ballistic factor.

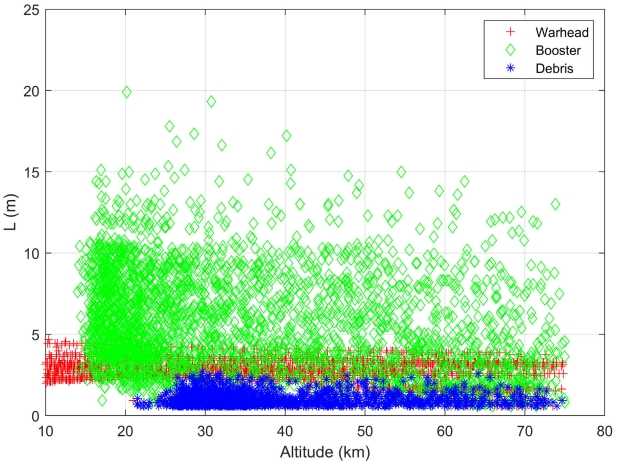

FIGURE 5. Estimated target length.

1) STEP 1

For training samples, the GFN models and their intersections for each attribute are shown in Fig. 6 and Fig. 7. Table 2 presents the GFN of corresponding propositions of each attribute.

2) STEP 2

For test samples, the mean and standard deviations are calculated using a one-dimensional KF. The test sample was selected from the warhead (W) class. Let $\eta_1 = 1.71 \times 10^{-3}$ m^2/kg and $\sigma_1 = 2.5 \times 10^{-4}$ m^2/kg for BF and $\eta_2 = 1.44$ m and $\sigma_2 = 0.15$ m for L. Table 3 presents the TFNs for the two examples. In Table 3, Example 1 shows that the models are formed, while reflecting uncertainty. Example 2 deals with the missing value. This implies that the track quality is poor, and the evidence becomes unreliable.

TABLE 1. Target parameters.

Class	Warhead	Booster	Debris	Heavy decoy
Shape	Conical	Cylinder	Flat-plate, Curve-plate, Cylinder	Conical
Diameter (m)	1.35–1.5	1.5	1.0–2.0	1.35
Length (m)	2.34–3.25	12.0–17.0	1.0–2.0	3.25
Ballistic Factor (m^2/kg)	1×10^{-4} to 4.5×10^{-4}	4×10^{-3} to 7×10^{-3}	3.5×10^{-2} to 8×10^{-2}	2.5×10^{-3}

TABLE 2. GFN for ballistic factor and length.

proposition	MF	GFN for BF ($k=1$)	GFN for L ($k=2$)
$\{\emptyset\}$	$\mu^k_{\tilde{\alpha}_0}(x)$	(0, 0, 0; 1)	(0, 0, 0; 1)
{W}	$\mu^k_{\tilde{\alpha}_1}(x)$	(2.26e-7, 1.00e-6, 3.00e-4, 2.43e-2; 1)	(0.39, 2.29, 4.88; 1)
{B}	$\mu^k_{\tilde{\alpha}_2}(x)$	(1.00e-4, 2.00e-3, 1.00e-2, 4.01e-2; 1)	(0.39, 4.60, 20.11; 1)
{D}	$\mu^k_{\tilde{\alpha}_3}(x)$	(8.00e-3, 3.00e-2, 1.00e-1, 1.00e-1; 1)	(0.39, 0.86, 2.89; 1)
{W,B}	$\mu^k_{\tilde{\alpha}_4}(x)$	(1.00e-4, 1.88e-3, 2.43e-2; 0.93)	(0.39, 3.17, 4.88; 0.66)
{W,D}	$\mu^k_{\tilde{\alpha}_5}(x)$	(8.00e-3, 1.58e-2, 2.43e-2; 0.35)	(0.39, 1.60, 2.89; 0.64)
{B,D}	$\mu^k_{\tilde{\alpha}_6}(x)$	(8.00e-3, 2.16e-2, 4.01e-2; 0.62)	(0.39, 2.08, 2.89; 0.40)
{W,B,D}	$\mu^k_{\tilde{\alpha}_7}(x)$	(8.00e-3, 1.58e-2, 2.43e-2; 0.35)	(0.39, 2.08, 2.89; 0.40)

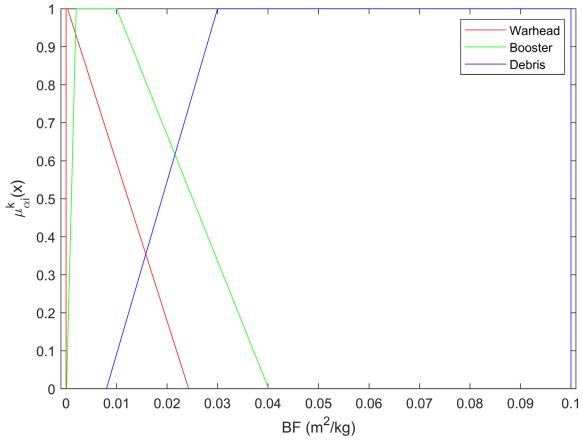

FIGURE 6. Membership function of ballistic factor.

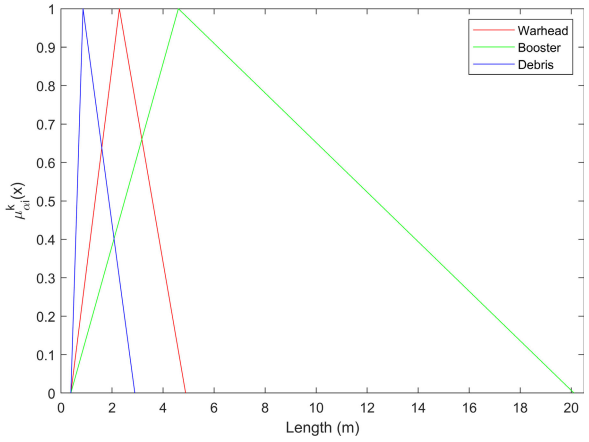

FIGURE 7. Membership function of target length.

TABLE 3. TFN for test samples.

Example	Attribute	TFN
Ex. 1	BF	(1.46e-3, 1.71e-3, 1.95e-3; 1)
($\sigma_k > \epsilon_k$)	L	(1.29, 1.44, 1.59; 1)
Ex. 2	BF	(1.46e-3, 1.71e-3, 1.95e-3; 1)
($\eta_k = 0$)	L	(0, 0, 0; 0)

TABLE 4. Normalized GBPA.

Attribute	GBPA	STEP 3 (Max.)	STEP 4 (Algorithm 1.)	STEP 4 (Normalize)
BF	$m(\alpha^1_0)$	0.000	0.000	0.000
	$m(\alpha^1_1)$	0.942	0.942	**0.522**
	$m(\alpha^1_2)$	0.864	0.000	0.000
	$m(\alpha^1_3)$	0.000	0.000	0.000
	$m(\alpha^1_4)$	0.864	0.864	**0.478**
	$m(\alpha^1_5)$	0.000	0.000	0.000
	$m(\alpha^1_6)$	0.000	0.000	0.000
	$m(\alpha^1_7)$	0.000	0.000	0.000
Length	$m(\alpha^2_0)$	0.000	0.000	0.000
	$m(\alpha^2_1)$	0.586	0.000	0.000
	$m(\alpha^2_2)$	0.275	0.000	0.000
	$m(\alpha^2_3)$	0.737	0.737	**0.461**
	$m(\alpha^2_4)$	0.275	0.000	0.000
	$m(\alpha^2_5)$	0.586	0.586	**0.367**
	$m(\alpha^2_6)$	0.275	0.000	0.000
	$m(\alpha^2_7)$	0.275	0.275	**0.172**

3) STEP 3 AND 4

Table 4 presents the calculation results for Example 1. For all propositions, the degree of support is calculated through (35) and (36). Using Algorithm 1, the conflicts between propositions are resolved. First, the largest $m(\alpha^2_3) = 0.737$ is selected, and $m(\alpha^2_1)$ and $m(\alpha^2_2)$ are removed for length attribute. Thereafter, $m(\alpha^2_4)$, $m(\alpha^2_6)$, and $m(\alpha^2_7)$ have the same value (0.275); hence, only $m(\alpha^2_7)$ remains. In this case, the removed proposition represents $\{W, B\}$ and $\{B, D\}$. The proposed method effectively yields a GBPA for proposition $\{W, B, D\}$ with many elements and removes the rest. Finally, a nested structure is formed based on the selected class. The same process is applied for the BF attribute. As a result, the GBPAs for the proposition $m(\{W\}) = 0.522$

TABLE 5. Intersection result for combining GBPA.

$m_1(B)m_2(C)$	$m(\{W\}) = 0.522$	m({W,B}) = 0.478
m({D}) = 0.461	$\{\emptyset\} = 0.241$	$\{\emptyset\} = 0.220$
m({W,D}) = 0.367	{W} = 0.192	{W} = 0.175
m({W,B,D}) = 0.172	{W} = 0.090	{W,B} = 0.082

and $m(\{W, B\}) = 0.478$ are supported by the BF attribute. For length, $m(\{D\}) = 0.461$, $m(\{W, D\}) = 0.367$, and $m(\{W, B, D\}) = 0.172$ are supported.

4) STEP 5

For decision-making, the combined GBPAs are calculated. In this step, a conflict occurs because the classes supported by the two attributes are different. The warhead class is supported by both attributes. However, the debris class is only supported by the length attribute. Table 5 presents the results of the intersection for combining the GBPAs.

The propositions of the debris for the length attribute do not intersect with the propositions for the BF attribute. Therefore, the combined GBPA for the debris is zero in (11). This means that the proposition of the D class is removed. Simultaneously, the conflict coefficient (K) is increased in (12). Finally, the warhead class is mainly supported by the combined GBPA ($m(\{W\}) = 0.848$, $m(\{W, B\}) = 0.152$, and $K = 0.461$). The conflict coefficient indicates the strength of the conflict between the evidence. As mentioned in STEP 5, we select the warhead class as a label with conflict coefficient. In a real application, this information is beneficial and helpful for final decision-making. As the results show, the TFN of Example 1 belongs to warhead class with the conflict coefficient, and it is matched with its actual class.

In Table 3, the missing length of Example 2 represents a lack of knowledge and it is considered an unknown class. For BF, the GBPAs are calculated as in Table 4. For length, only $m(\alpha_0^2) = 1$ can be assigned according to $1 - \sum_{i=1}^{m} m(\alpha_i^k)$ in STEP 4. The final GBPA was calculated only for $m(\alpha_0) = 1$. In this case, the result of GBPAs is reported without a target label. The proposed algorithm can also effectively represent conflicts between evidence that may occur in real applications.

VI. SIMULATION

A. COMPARISON WITH WELL-KNOWN CLASSIFIER

The proposed method was compared with a well-known classifier, such as Naive Bayes, ensemble, k-Nearest Neighbor (KNN), and support vector machine (SVM). The five-fold cross-validation was performed to select the classifier. The classifiers were selected based on high validation accuracy as follows: Ensemble (97.6 %), KNN (96.0 %), Naive Bayes (95.7 %), and SVM (95.7 %). These classifiers are feasible in a complete FOD. In this case, the proposed algorithm has downward compatibility with D-S theory [17]. Under these assumptions, we use the pignistic probability to obtain the label with the parameter $\epsilon_0 = 0.0001$ in STEP 3. In addition, the proposed method was compared with the existing method of using the mean and k-means++ clustering for the center of the TFN, as mentioned in STEP 1.

Table 6 represents the classification accuracy, which is the rate of correct classifications of the proposed method and those of others. The warhead classification accuracy of the SVM was the highest, whereas the classification accuracy of the booster was the lowest. Because the booster training samples are widely spread out, the samples can be trained to be included in the warhead class in Figs. 4–5. This may result in an insufficient margin of the SVM. The booster can have more test samples beyond the decision boundaries than the warhead samples. Therefore, false alarms may occur in the booster test samples. Similarly, the results of the k-means++ clustering method also reveal the low classification accuracy of the booster. This may occur because the clustering method only considers the distances, and not the densities. In addition, the clustering method only utilizes the raw data without the target label. Each sample in the data set is obtained from a known target label. Therefore, there is an obvious method for grouping the data. In our experiment, the classification accuracy was better than that for k-means++ clustering when the mean of the each group was used as the center of the TFN. The proposed method uses the GFN and the TFN to encode the data distribution and also utilizes the typical values. The classification accuracy of the proposed algorithm is 94.2 % on average, representing the best results. In addition, the classification accuracy of the booster becomes 90.8 %. The high classification accuracy implies that the proposed method is effective in determining the GBPA and classifying the correct class.

In particular, fast and stable classification performance is important for intercepting warhead at high altitudes. Figs. 8–10 present the results for the average time. The time-averaged classification accuracy represents the proportion of correctly classified targets for each tracking time slot. The minimum classification time is selected based on the time the classifier no longer misclassifies the actual class after that time. In Fig. 8, the minimum time of the proposed method without leakage is 8.83 s, which is less than that of the SVM (i.e., 9.68 s). Classifiers other than Bayes increase the classification accuracy faster than the proposed method, but over time, they suffer from some leakages. This indicates the possibility of misclassification for warheads at low altitude. The leakage is a fatal drawback. The performance of the proposed method was verified to be excellent in terms of maintaining stable classification results for warhead engagement. As shown in Fig. 9, the proposed method stably classifies booster after 21.67 s, but Bayes stabilizes after 34.42 s. Fig. 10 shows that, at 84.83 s, all methods indicate a false alarm, but most accurately classify the debris in the entire target scenario. The results of Fig. 9 and 10 indicate that there is sufficient time to remove the booster and debris in advance.

Table 7 summarizes the minimum time without leakage or false alarm. The results indicate that the proposed method can classify the warhead faster than the other methods

TABLE 6. Classification accuracy (%).

Class	Bayes	Ensemble	KNN	SVM	TFN (mean)	TFN (k-means++)	**Ours** (GFN + TFN)
Warhead	75.9	91.7	92.4	**96.1**	92.2	91.1	92.6
Booster	89.4	88.4	86.9	64.6	81.7	71.7	**90.8**
Debris	99.2	98.5	99.2	98.9	99.2	99.2	**99.2**
Average	88.2	92.9	92.8	86.5	91.0	87.3	**94.2**

TABLE 7. Minimum time without leakage or false alarm (s).

Class	Bayes	Ensemble	KNN	SVM	TFN (mean)	TFN (k-means++)	**Ours** (GFN + TFN)
Warhead	28.09	38.44	14.48	9.68	10.50	10.50	**8.83**
Booster	34.42	36.00	38.43	45.61	38.43	44.80	**21.67**
Debris	84.83	84.83	84.83	84.83	84.83	84.83	**84.83**

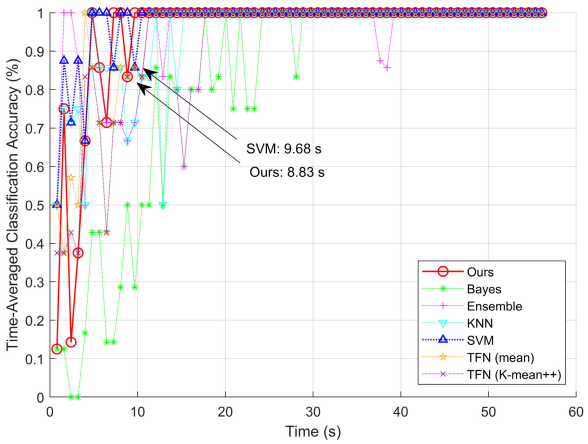

FIGURE 8. Minimum classification time for warhead.

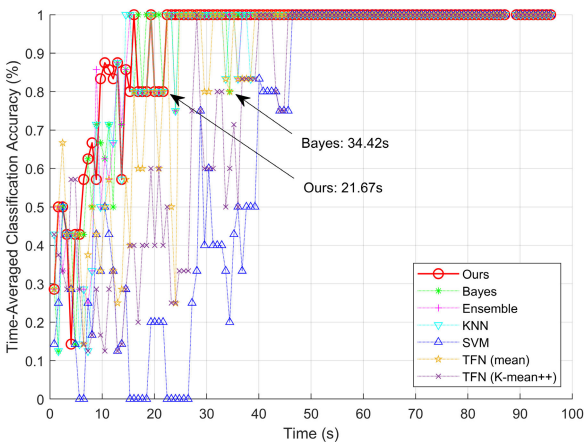

FIGURE 9. Minimum classification time for booster.

and eliminate non-warhead by reducing the number of false alarms.

B. COMPARISON WITH DIFFERENT UNCERTAINTY

In this section, we analyze the influence of the input uncertainty on the classification results. The proposed algorithm was compared with the method using a single test data.

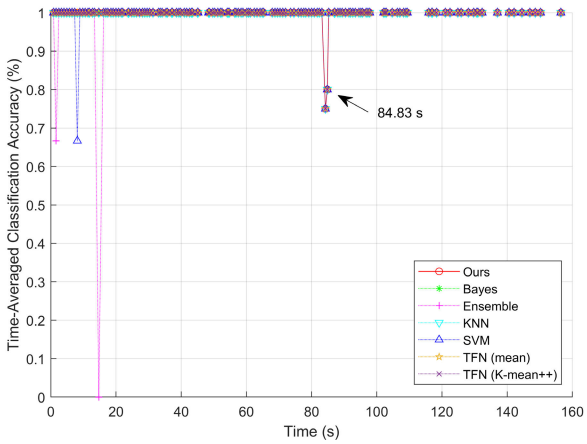

FIGURE 10. Minimum classification time for debris.

To analyze the effect of uncertainty, the combined GBPA was calculated for a warhead test class while varying κ_j in (34). In this experiment, only κ_j determines the amount of input uncertainty. In Fig. 11 the dashed line represents a single value ($0 \cdot \sigma_k$), the solid line represents $\pm 1 \cdot \sigma_k$, the dash-dot line represents $\pm 2 \cdot \sigma_k$, and the dotted line represents $\pm 3 \cdot \sigma_k$.

First, assuming there is no uncertainty, the proposed method behaves similarly to the method using single values. In this case, the uncertainty was ignored. This is because the existing methods treat the input as a single deterministic value. Therefore, the value of κ_j is set to zero. In Fig. 11, a high value is assigned to $m(\{D\})$ represented by blue dashed line at approximately 3.0 s. However, because the radar input uncertainty was ignored, a high GBPA value does not always guarantee high classification accuracy. In the early stages of tracking, the BF and L values of the warhead can vary significantly, and it takes them time to converge. In Fig. 4, the BF value of the warhead can be estimated up to approximately 0.025 m^2/kg. Similarly, the length of the warhead can be estimated in the length area of the debris in Fig. 5. The existing methods assume that the radar input has no uncertainty and is always accurate. As a result, the debris class can be selected with a high combined GBPA. This can lead to a leakage or false alarms in real environments.

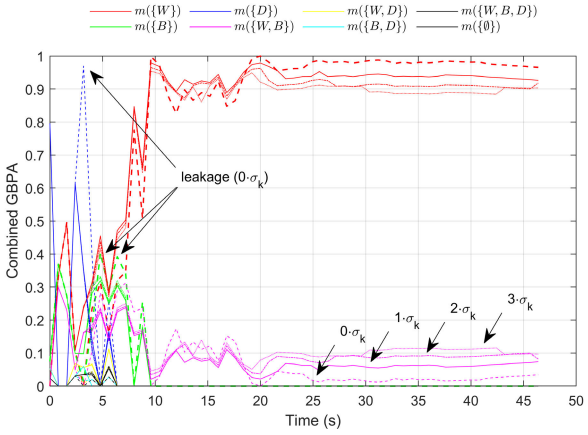

FIGURE 11. Combined GBPAs for each sigma.

The proposed method encodes the input uncertainty into the TFN and allows the GBPA to be assigned to other propositions. The GCR denotes that all the GBPAs from each attribute are reflected and normalized. As a result, the proposed method reduces the $m(\{D\})$ to less than 0.5 at 3.0 s. A similar leakage, represented by the green dashed line, that classifies the warhead as a booster is also observed at 4.9 s and 6.4 s; however, the proposed method did not classify the warhead as a booster. This result is reflected in the classification accuracy. The combined GBPA may have a high value if the input uncertainty is ignored, but the average classification accuracy is 92.6 %, which is the lowest in Table 8.

Second, we only increased the κ_j to analyze the influence of the radar input uncertainty in the same test scenario. For explanation purposes, when BF and L support $m(\{W\})$ and $m(\{B\})$, respectively, with the highest probability, input uncertainty can reduce conflict by allowing GBPA to be assigned to other propositions. However, the input uncertainty also increases the uncertainty of the information. At this time, the increased uncertainty of the information is reflected in the GBPAs which represent the degree of belief. For example, we assume that the BF is estimated stably in the warhead area. The estimated mean of the length was 4.5 m, and the standard deviation was 0.5 m in the booster area. In Fig. 7, the increased κ_j can increase the maximum value of the intersection area for the proposition $\{W, B\}$. This indicates the degree of belief of the $m(\{W, B\})$ is increased. The proposed method decreases the $m(\{W\})$ for the proposition of warhead class, as the constant value κ_j multiplied by sigma increases in Fig. 11. In contrast, the $m(\{W, B\})$ increases among the remaining propositions. This indicates that the input uncertainty can reduce the combined belief that supports proposition $\{W\}$. Simultaneously, the input uncertainty increased the ambiguity by increasing the combined belief that supports proposition $\{W, B\}$, which denotes either the warhead or the booster. This is reasonable because the higher the radar input uncertainty, the less likely it is to be a target. Fig. 11 shows that the input uncertainty was effectively reflected in the GBPAs.

TABLE 8. Classification accuracy for sigma (%).

Class	Ours			
	$0 \cdot \sigma_k$	$\pm 1 \cdot \sigma_k$	$\pm 2 \cdot \sigma_k$	$\pm 3 \cdot \sigma_k$
Warhead	87.8	**92.6**	92.2	92.4
Booster	90.8	**90.8**	90.0	88.5
Debris	99.2	**99.2**	98.9	98.9
Average	92.6	**94.2**	93.7	93.3

Table 8 summarizes the classification accuracy according to κ_j values for the entire test samples. The magnitude of the input uncertainty can affect the classification results. The results show that the average classification accuracy decreased with increasing uncertainty in radar inputs. The average classification accuracy was the lowest even though the highest GBPA was assigned when uncertainty was ignored. Our experiments show that $1 \cdot \sigma_k$ affords the best results for all target classes.

C. UNCERTAIN TARGET

In a real attack, the attacker might release dozens of decoys while disguising the appearance of the warhead. In this case, the radar cannot be expected to collect a priori information that can allow the classifier to identify the objects [54]. In this section, we consider objects that are not defined in the FOD, such as decoys.

The air resistance increases in the reentry phase. Therefore, we assume that the light decoy balloons can be differentiated from the warhead. However, the heavy decoy that was released alongside the warhead can affect the classification performance. We assumed that the heavy decoy was the target of a warhead-like motion. The heavy decoy is an anonymous class, but it is not represented as an empty set because the measured values are in the FOD. This is an example of incomplete knowledge of the target class. We simulated the BF and length features of the heavy decoy based on two assumptions. First, we assumed that the heavy decoy had a mock warhead shape, and that there was a random rotational motion, such as tumbling, in the reentry phase. Therefore, the estimated target length would fluctuate and depend strongly on the aspect angle of the radar. Second, we assumed that the BF was initially similar to a warhead but approached the booster area over time owing to irregular motion and air resistance.

Figs. 12–13 present the length and BF attributes of the heavy decoy, respectively. The BF was simulated between the warhead and the booster area, and the length was simulated in the areas of the warhead, booster, and debris.

The results are compared to the warhead test scenario presented in Fig. 11. To analysis the results, $1 \cdot \sigma_k$ and the conflict coefficient (K) were used. Figs. 14–15 present the combined GBPAs and K for the heavy decoy and the warhead, respectively. As the heavy decoy mainly has a warhead-like motion, proposition $\{W\}$ is supported by Fig. 14. However, the conflict coefficient (K) increased for the heavy decoy. The $m(\{W\})$, which represents the degree of belief, decreased over time. In this case, the conflict coefficient can be used as information that indicates an uncertain target. In contrast,

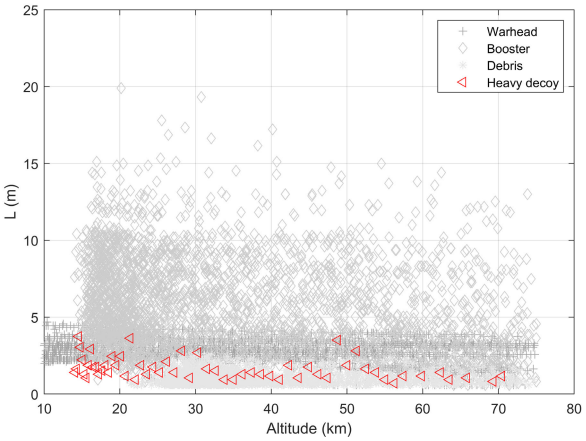

FIGURE 12. Estimated target length of the heavy decoy.

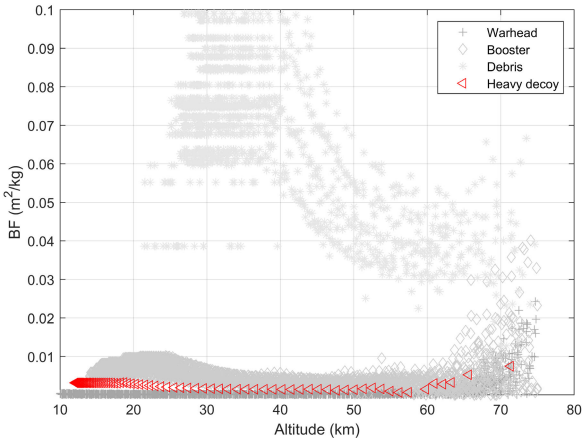

FIGURE 13. Estimated ballistic factor of the heavy decoy.

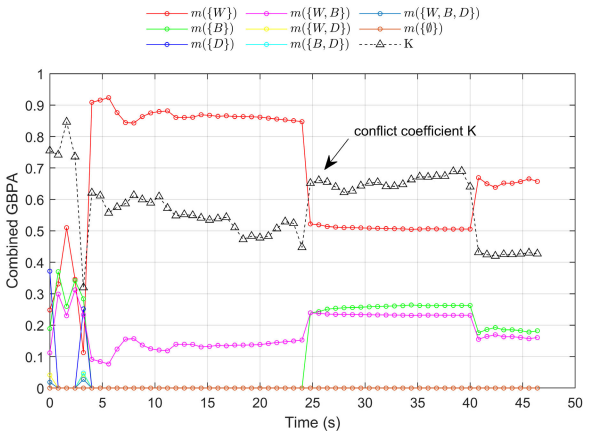

FIGURE 14. Combined GBPAs and K for the heavy decoy.

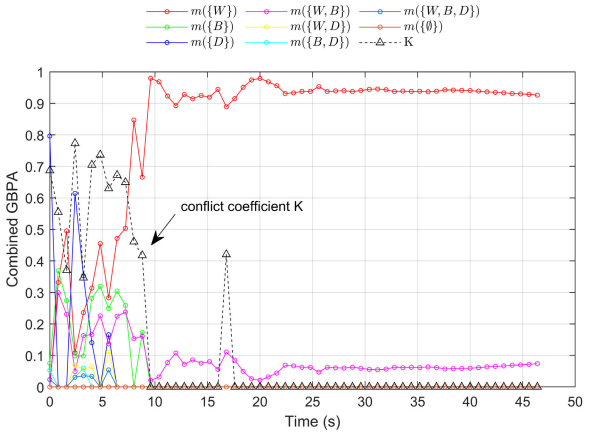

FIGURE 15. Combined GBPAs and K for the warhead.

in Fig. 15, the $m(\{W\})$ gradually increased and remained above 0.9. The conflict coefficient became zero, indicating that there is no conflict of evidence. The proposed method can report the reliability for the target label by providing K to the C2 system. The proposed method can also effectively represent the conflicts between evidence that may arise from the attributes of the uncertain target without a priori information. The difficulty of target classification increases in the open world, where undefined classes exist. However, until recently, defense tests did not include the realistic decoys that the system is expected to face in the open world [54]. Therefore, this information with K may not be sufficient, and more features may be required. In a multi-layered BMD system, the C2 system can fuse various pieces of sensor information. The final decision of the C2 system is beyond the scope of this study and remains a topic for future research.

D. DISCUSSION

In this section, we discuss the contribution of the proposed method from the perspective of determining GBPA. The proposed TFN encoding method can effectively reflect the input uncertainty to the GBPA. This feature distinguishes the proposed method from existing methods. If the input uncertainty is sufficiently small, the proposed method determines GBPA using the intersection points and achieves downward compatibility. If the target is tracked with identical values but exhibits different tracking errors, the proposed method efficiently reflects the input uncertainty to the GBPA, respectively. On the contrary, the existing methods ignore the uncertainty and generate the same GBPA, thereby undermining the reliability of the classifier for each input uncertainty.

VII. CONCLUSION

In this paper, we proposed a novel method for determining the GBPA based on the GFN and the TFN to reflect the input uncertainty in the open world. Owing to the military environment, the radar sensor input might be cluttered with noise, and undefined targets may exist. The proposed method presents a promising alternative to handling uncertainty when determining GBPA and outperforms other methods over datasets with the warheads, boosters, and debris. Based on the experiments and results of this paper, the proposed method achieves fast and stable classification performance. The results demonstrate that our method can accurately and effectively determine the GBPA. Furthermore, the simulation results verify that the proposed TFN encoding method

can effectively reflect the input uncertainty to the combined GBPA. In addition, the conflict coefficient provides additional information about uncertain or unknown targets in the incomplete FOD. This is an advantage as it is different from the information provided by the existing classifiers in the complete FOD. The proposed method can reflect the radar tracking quality and measurement uncertainty to the classification results and can be flexibly extended for many engineering applications. Considering the theoretical and practical applications, we will focus on increasing the data set and finding useful features for classification in the open world as future research.

REFERENCES

[1] A. R. Persico, C. V. Ilioudis, C. Clemente, and J. J. Soraghan, "Novel classification algorithm for ballistic target based on HRRP frame," *IEEE Trans. Aerosp. Electron. Syst.*, vol. 55, no. 6, pp. 3168–3189, Dec. 2019.

[2] G. N. Lewis, "Ballistic missile defense effectiveness," in *Proc. AIP Conf.*, 2017, vol. 1898, no. 1, Art. no. 030007.

[3] A. G. Huizing and A. A. F. Bloemen, "An efficient scheduling algorithm for a multifunction radar," in *Proc. Int. Symp. Phased Array Syst. Technol.*, Oct. 1996, pp. 359–364.

[4] K. Coombs, D. Freel, D. Lampert, and S. J. Brahm, "Using Dempster-Shafer methods for object classification in the theater ballistic missile environment," *Proc. SPIE*, vol. 3719, pp. 103–113, Mar. 1999.

[5] A. R. Persico, C. Clemente, D. Gaglione, C. V. Ilioudis, J. Cao, L. Pallotta, A. De Maio, I. Proudler, and J. J. Soraghan, "On model, algorithms, and experiment for micro-Doppler-based recognition of ballistic targets," *IEEE Trans. Aerosp. Electron. Syst.*, vol. 53, no. 3, pp. 1088–1108, Jun. 2017.

[6] B. Rao, Y.-L. Zhao, S.-P. Xiao, and X.-S. Wang, "Discrimination of exo-atmospheric active decoys using acceleration information," *IET Radar, Sonar Navigat.*, vol. 4, no. 4, pp. 626–638, 2010.

[7] K. W. Yoo, J. H. Chun, and B. G. Choi, "Target classification and tracking based on aerodynamic properties and RCS information using Rao-Blackwellized particle filter," in *Proc. Photon. Electromagn. Res. Symp.-Fall (PIERS-Fall)*, Dec. 2019, pp. 146–154.

[8] U. K. Singh, V. Padmanabhan, and A. Agarwal, "Dynamic classification of ballistic missiles using neural networks and hidden Markov models," *Appl. Soft Comput.*, vol. 19, pp. 280–289, Jun. 2014.

[9] A. Bhattacharyya, V. K. Saraswat, P. Manimaran, and S. B. Rao, "Evidence theoretic classification of ballistic missiles," *Appl. Soft Comput.*, vol. 37, pp. 479–489, Dec. 2015.

[10] P. Mehta, A. De, D. Shashikiran, and K. P. Ray, "Radar target classification using improved Dempster–Shafer theory," *J. Eng.*, vol. 2019, no. 21, pp. 7872–7875, Nov. 2019.

[11] J. Chen, S. Xu, and Z. Chen, "Convolutional neural network for classifying space target of the same shape by using RCS time series," *IET Radar, Sonar Navigat.*, vol. 12, no. 11, pp. 1268–1275, Nov. 2018.

[12] W. Tang, L. Yu, Y. Wei, and P. Tong, "Radar target recognition of ballistic missile in complex scene," in *Proc. IEEE Int. Conf. Signal, Inf. Data Process. (ICSIDP)*, Dec. 2019, pp. 1–6.

[13] A. R. Persico, C. Ilioudis, C. Clemente, and J. Soraghan, "Novel approach for ballistic targets classification from HRRP frame," in *Proc. Sensor Signal Process. Defence Conf. (SSPD)*, Dec. 2017, pp. 1–5.

[14] Y. Wang, C. Feng, Y. Zhang, and S. He, "Space precession target classification based on radar high-resolution range profiles," *Int. J. Antennas Propag.*, vol. 2019, pp. 1–9, Feb. 2019.

[15] S. Hui-xia, L. Zheng, and X. Ning, "Ballistic missile warhead recognition based on micro-Doppler frequency," *Defence Sci. J.*, vol. 58, no. 6, pp. 705–709, Nov. 2008.

[16] K. Y. Guo and X. Q. Sheng, "A precise recognition approach of ballistic missile warhead and decoy," *J. Electromagn. Waves Appl.*, vol. 23, nos. 14–15, pp. 1867–1875, Jan. 2009.

[17] J. Zhang and Y. Deng, "A method to determine basic probability assignment in the open world and its application in data fusion and classification," *Appl. Intell.*, vol. 46, no. 4, pp. 934–951, Jun. 2017.

[18] Y. Deng, "Uncertainty measure in evidence theory," *Sci. China Inf. Sci.*, vol. 63, no. 11, pp. 1–19, Nov. 2020.

[19] R. Sun and Y. Deng, "A new method to determine generalized basic probability assignment in the open world," *IEEE Access*, vol. 7, pp. 52827–52835, 2019.

[20] L. Changxi, Z. Yan, and L. Han, "A new method of ballistic mission target recognition," in *Proc. Joint. Int. Mech., Electron. Inf. Technol. Conf.* Atlantis Press, Dec. 2015, pp. 298–306. [Online]. Available: https://www.atlantis-press.com/proceedings/jimet-15/25843771, doi: 10.2991/jimet-15.2015.55.

[21] Y. Deng, "Generalized evidence theory," *Appl. Intell.*, vol. 43, no. 3, pp. 530–543, Oct. 2015.

[22] W. Jiang, J. Zhan, D. Zhou, and X. Li, "A method to determine generalized basic probability assignment in the open world," *Math. Problems Eng.*, vol. 2016, May 2016, Art. no. 3878634.

[23] F. Liu and Y. Deng, "Determine the number of unknown targets in open world based on elbow method," *IEEE Trans. Fuzzy Syst.*, early access, Jan. 13, 2020, doi: 10.1109/tfuzz.2020.2966182.

[24] P. Xu, X. Su, S. Mahadevan, C. Li, and Y. Deng, "A non-parametric method to determine basic probability assignment for classification problems," *Appl. Intell.*, vol. 41, no. 3, pp. 681–693, Oct. 2014.

[25] B. Qin and F. Xiao, "A non-parametric method to determine basic probability assignment based on kernel density estimation," *IEEE Access*, vol. 6, pp. 73509–73519, 2018.

[26] P. Xu, Y. Deng, X. Su, and S. Mahadevan, "A new method to determine basic probability assignment from training data," *Knowl.-Based Syst.*, vol. 46, pp. 69–80, Jul. 2013.

[27] L. Fei, J. Xia, Y. Feng, and L. Liu, "A novel method to determine basic probability assignment in Dempster–Shafer theory and its application in multi-sensor information fusion," *Int. J. Distrib. Sensor Netw.*, vol. 15, no. 7, pp. 1–16, 2019.

[28] H. X. Li, Y. Wang, and C. L. P. Chen, "Dempster–Shafer structure based fuzzy logic system for stochastic modeling," *Appl. Soft Comput.*, vol. 56, no. 1, pp. 134–142, Jul. 2017.

[29] W. Jiang, Y. Yang, Y. Luo, and X. Qin, "Determining basic probability assignment based on the improved similarity measures of generalized fuzzy numbers," *Int. J. Comput. Commun. Control*, vol. 10, no. 3, pp. 333–347, 2015.

[30] Y. Li, D. Pelusi, and Y. Deng, "Generate two-dimensional belief function based on an improved similarity measure of trapezoidal fuzzy numbers," *Comput. Appl. Math.*, vol. 39, no. 4, pp. 1–20, Dec. 2020.

[31] T. Ma and F. Xiao, "An improved method to transform triangular fuzzy number into basic belief assignment in evidence theory," *IEEE Access*, vol. 7, pp. 25308–25322, 2019.

[32] L. Pan and Y. Deng, "An association coefficient of a belief function and its application in a target recognition system," *Int. J. Intell. Syst.*, vol. 35, no. 1, pp. 85–104, Jan. 2020.

[33] G. Welch and G. Bishop, "An introduction to the Kalman filter," Dept. Comput. Sci., Univ. North Carolina, Tech. Rep. TR 95-041, 1995.

[34] K.-Y. Jung, "Performance analysis of tactical ballistic missile tracking filters in phased array multi-function radar," *J. Korean Inst. Electromagn. Eng. Sci.*, vol. 23, no. 8, pp. 995–1001, Aug. 2012.

[35] P. Dodin, P. Minvielle, and J. P. L. Cadre, "Estimating the ballistic coefficient of a re-entry vehicle," *IET Radar, Sonar Navigat.*, vol. 1, no. 3, pp. 173–183, Jun. 2007.

[36] L. Du, H. Liu, Z. Bao, and M. Xing, "Radar HRRP target recognition based on higher order spectra," *IEEE Trans. Signal Process.*, vol. 53, no. 7, pp. 2359–2368, Jul. 2005.

[37] X. Ai, X. Zou, Y. Li, J. Yang, and S. Xiao, "Bistatic scattering centres of cone-shaped targets and target length estimation," *Sci. China Inf. Sci.*, vol. 55, no. 12, pp. 2888–2898, Dec. 2012.

[38] X. Ai, Y. Li, X. Wang, and S. Xiao, "Some results on characteristics of bistatic high-range resolution profiles for target classification," *IET Radar, Sonar Navigat.*, vol. 6, no. 5, pp. 379–388, Jun. 2012.

[39] G.-G. Choi, S.-K. Han, H.-J. Jo, H.-T. Kim, K.-T. Kim, S.-C. Song, and Y.-J. Na, "A study on signal processing of ballistic missile warhead discrimination using ESPRIT in millimeter-wave(Ka-band) seeker," *J. Korean Inst. Electromagn. Eng. Sci.*, vol. 23, no. 2, pp. 266–269, Feb. 2012.

[40] G. Forden, "Gui_missile_flyout: A general program for simulating ballistic missiles," *Sci. Global Secur.*, vol. 15, no. 2, pp. 133–146, 2007.

[41] A. P. Dempster, "Upper and lower probabilities induced by a multivalued mapping," in *Classic Works of the Dempster-Shafer Theory of Belief Functions*. Berlin, Germany: Springer, 2008, pp. 57–72.

[42] G. Shafer, *A Mathematical Theory of Evidence*. Princeton, NJ, USA: Princeton Univ. Press, 1976.

[43] F. Xiao, "An improved method for combining conflicting evidences based on the similarity measure and belief function entropy," *Int. J. Fuzzy Syst.*, vol. 20, no. 4, pp. 1256–1266, Apr. 2018.
[44] P. Smets and R. Kennes, "The transferable belief model," *Artif. Intell.*, vol. 66, no. 2, pp. 191–234, Apr. 1994.
[45] L. A. Zadeh, "Fuzzy sets," *Inf. Control*, vol. 8, no. 3, pp. 338–353, Jun. 1965.
[46] S.-H. Chen, "Ranking fuzzy numbers with maximizing set and minimizing set," *Fuzzy Sets Syst.*, vol. 17, no. 2, pp. 113–129, Nov. 1985.
[47] P. Dutta, "Uncertainty modeling in risk assessment based on Dempster–Shafer theory of evidence with generalized fuzzy focal elements," *Fuzzy Inf. Eng.*, vol. 7, no. 1, pp. 15–30, Mar. 2015.
[48] S.-M. Chen and J.-H. Chen, "Fuzzy risk analysis based on ranking generalized fuzzy numbers with different heights and different spreads," *Expert Syst. Appl.*, vol. 36, no. 3, pp. 6833–6842, Apr. 2009.
[49] S.-M. Chen, A. Munif, G.-S. Chen, H.-C. Liu, and B.-C. Kuo, "Fuzzy risk analysis based on ranking generalized fuzzy numbers with different left heights and right heights," *Expert Syst. Appl.*, vol. 39, no. 7, pp. 6320–6334, Jun. 2012.
[50] K. R. Moon, T. H. Kim, and T. L. Song, "Comparison of ballistic-coefficient-based estimation algorithms for precise tracking of a re-entry vehicle and its impact point prediction," *J. Astron. Space Sci.*, vol. 29, no. 4, pp. 363–374, Dec. 2012.
[51] A. Farina, M. G. D. Gaudio, U. D'Elia, S. Immediata, L. Ortenzi, L. Timmoneri, and M. R. Toma, "Detection and tracking of ballistic target," in *Proc. IEEE Radar Conf.*, Apr. 2004, pp. 450–456.
[52] R. Savelsberg, "An analysis of North Korea's satellite launches," *J. Mil. Stud.*, vol. 3, no. 1, pp. 31–54, Dec. 2012.
[53] R. Schmidt, "Multiple emitter location and signal parameter estimation," *IEEE Trans. Antennas Propag.*, vol. 34, no. 3, pp. 276–280, Mar. 1986.
[54] D. Wright, "Decoys used in missile defense intercept tests, 1999–2018," Tech. Rep., Apr. 2019. [Online]. Available: http://www.jstor.org/stable/resrep24116

KWANGYONG JUNG was born in Seoul, South Korea, in 1979. He received the B.S. and M.S. degrees in electronic and computer engineering from Hanyang University, Ansan, South Korea, in 2005 and 2007, respectively. He is currently pursuing the Ph.D. degree in electrical and electronic engineering with Yonsei University, Seoul.

From 2006 to 2012, he worked as a Radar Software Engineer with the Radar System Group, Samsung Thales Company Ltd., South Korea. Since 2013, he has been working as a Radar System Engineer with the Land Radar Team, Hanwha Systems Company Ltd., South Korea. His research interests include target tracking, machine learning, deep learning, and their application to radar systems.

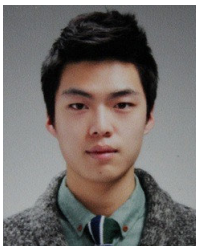

SAWON MIN was born in Seoul, South Korea, in 1991. He received the B.S. degree in electronic engineering from Chung-Ang University, Seoul, in 2015.

Since 2016, he has been working as a Radar Software Engineer with the Land Radar Team, Hanwha Systems Company Ltd., South Korea. His research interests include modeling and simulation, and their application to radar systems.

JEONGWOO KIM was born in Boeun, South Korea, in 1985. He received the B.S. and M.S. degrees in electronic engineering from Chungbuk University, Cheongju, South Korea, in 2010 and 2012, respectively.

From 2012 to 2016, he was a Wi-Fi System Engineer with INC Technology Company Ltd., South Korea. Since 2016, he has been working as a Radar System Engineer with the Land Radar Team, Hanwha Systems Company Ltd., South Korea. His research interests include radar performance analysis, and their application to radar systems.

NAMMOON KIM was born in Boeun, South Korea, in 1982. He received the B.S., M.S., and Ph.D. degrees in electronic engineering from Kwangwoon University, Seoul, South Korea, in 2011 and 2016, respectively.

Since 2016, he has been working as a Radar System Engineer with the Land Radar Team, Hanwha Systems Company Ltd., South Korea. His research interests include indoor navigation, and radar performance analysis.

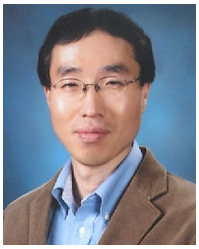

EUNTAI KIM (Member, IEEE) was born in Seoul, South Korea, in 1970. He received the B.S., M.S., and Ph.D. degrees in electronic engineering from Yonsei University, Seoul, in 1992, 1994, and 1999, respectively.

From 1999 to 2002, he was a full-time Lecturer with the Department of Control and Instrumentation Engineering, Hankyong National University, South Korea. Since 2002, he has been a Faculty Member with the School of Electrical and Electronic Engineering, Yonsei University, where he is currently a Professor. He was also a Visiting Researcher with the Berkeley Initiative in Soft Computing, University of California, Berkeley, Berkeley, CA, USA, in 2008. His current research interests include computational intelligence, statistical machine learning and deep learning and their application to intelligent robotics, autonomous vehicles, and robot vision.